Position- and momentum-space two-body correlations in a weakly interacting trapped condensate

Salvatore Butera,[1] David Clément,[2] and Iacopo Carusotto[3]
[1]*School of Physics and Astronomy, University of Glasgow, Glasgow G12 8QQ, United Kingdom*
[2]*Université Paris Saclay, Institut d'Optique Graduate School, CNRS, Laboratoire Charles Fabry, 91127 Palaiseau, France*
[3]*INO-CNR BEC Center and Dipartimento di Fisica, Università di Trento, I-38123 Povo, Italy*

(Received 31 August 2020; revised 27 November 2020; accepted 15 December 2020; published 4 January 2021)

We investigate the position- and momentum-space two-body correlations in a weakly interacting, harmonically trapped atomic Bose-Einstein condensed gas at low temperatures. The two-body correlations are computed within the Bogoliubov approximation and the consequences of the finite system size are highlighted in contrast to the spatially homogeneous case. In the position space, we recover the antibunching induced by the repulsive interatomic interaction in the condensed fraction localized around the trap center and the bunching in the outer thermal cloud. In the momentum space, bunching signatures appear for either equal or opposite values of the momentum and display peculiar features as a function of the momentum and the temperature. In analogy to the optical Hanbury-Brown and Twiss effect, the amplitude of the bunching signal at closeby momenta is fixed by the chaotic nature of the matter field state and its linewidth is shown to be set by the (inverse of the) finite spatial size of the associated in-trap momentum components. In contrast, the linewidth of the bunching signal at opposite momenta is only determined by the condensate size.

DOI: 10.1103/PhysRevA.103.013302

I. INTRODUCTION

Correlation functions are among the most powerful tools to characterize the properties of light beams in quantum optics and to access the microscopic structure of condensed matter systems. In the former context, the distinction between thermal light (a lamp) versus coherent light (a laser) and single-photon source (a single two-level emitter) is typically made by looking at the Glauber coherence functions via the statistical properties of suitable photodetection signals [1,2]. In the latter context, proximity to a critical point and the onset of an ordered phase are typically encoded in the correlation functions of the order parameter, namely the local magnetization (for the ferromagnetic transition [3]) or the Bose field (for the Bose-Einstein condensation transition [4–7]).

In spatially large systems, position-space correlations between local observables are typically determined by the bulk properties of the system and are only weakly affected by its unavoidably finite size and the presence of edges. The situation is completely different for what concerns correlation functions in the reciprocal space, e.g., between different momentum states. The Fourier transform relating position and momentum spaces is in fact a strongly nonlocal operation and, as such, is strongly affected by the overall size of the system.

The most celebrated example in this sense are the Hanbury-Brown and Twiss (HB-T) correlations between different momentum states of an atomic cloud [8–14]. These studies were inspired by pioneering quantum optics experiments exploiting a subtle relation between the spatial profile of the intensity correlation function of the light detected on Earth and the angular size of a remote star [15]. Along similar lines, the momentum-space correlation function of the atoms showed a nontrivial bunching signal with a momentum-space linewidth determined by the overall size of the cloud. This is to be contrasted with the typical δ-shaped form of momentum-space correlations of spatially infinite and homogeneous systems.

While first works on matter wave HB-T physics were restricted to the simplest case of noninteracting atoms of either bosonic [8,10,12] or fermionic [16] nature, recent developments have started investigating the richer physics of interacting gases. In such systems, the excitation modes have a collective nature and sizable quantum correlations among the elementary constituents are present in the many-body ground state [17–20]. On one hand, it is natural that signatures of these many-body properties of the bulk should be well visible in the position- and momentum-space correlation functions. On the other hand, we can also expect that the detailed structure of the momentum dependence of the correlation function should keep memory of the overall size of the system and possibly of its spatial shape.

Motivated by the recent experiment [21], in this work we report a complete theoretical study of such finite-size effects in a simplest model of many-body system that is amenable to *ab initio* numerical calculations and analytical insight, but at the same time is rich enough to display a nontrivial physics. We consider a gas of weakly interacting bosonic particles in the presence of a harmonic trapping potential [20]. At low temperatures, this system can be described within the Bogoliubov theory based on a macroscopically occupied Bose-Einstein condensate (BEC) and a set of noninteracting bosonic excitation modes, whose nature spans from low-energy collective modes to high-energy single-particle states [22]. At finite temperature, the thermal population of these

excitation modes gives rise to the thermal cloud. Because of interactions, the ground state also contains a sizable quantum depletion, formed by pairs of particles that are excited out of the condensate by virtual two-body collision processes into states with exactly opposite momenta.

While this picture holds in spatially infinite and homogeneous condensates, several mechanisms were shown to introduce additional features in the momentum space correlation pattern, from quasicondensation effects in reduced dimensions [23] to different states of bosonic matter in optical lattices [24]. Here we specifically focus on the consequences of the finite size of a dilute condensate on the linewidth of the different features in the correlation pattern in momentum space. Inspired by the Hanbury-Brown and Twiss argument, one of the goals of this work is to assess the relation between the momentum-space linewidth to the inverse physical size of the system as recently explored in Ref. [21].

In order to achieve the momentum-space selectivity and condensate size values that are required to access the fine details of the Hanbury-Brown and Twiss physics, we choose to focus on one-dimensional (1D) geometries. Those quasicondensation features that are typical of low-dimensional systems are suppressed by working deep in the weakly interacting limit. For the rest, we do not expect that any new physics is introduced into the problem when increasing the dimension of the system to 2D or 3D. This statement appears to be confirmed by the recent experiment [21].

The structure of the work is the following. In Sec. II, we present the physical system under consideration (Sec. II), and we review the basic concepts of the Bogoliubov approximation (Secs. II B and II C). These well-known facts are the basis for our study of the spatial shape of the Bogoliubov modes in trapped geometries that is reported in Sec. II D. The general theory of two-body correlations within the Bogoliubov approach is reviewed in Sec. III and its application to spatially homogeneous systems is summarized in Sec. IV.

Section V presents the main results of our work. The interplay of quantum antibunching features due to interactions with the bunching features due to the thermal cloud are highlighted in the real-space correlations discussed in Sec. V A. The role of the finite system size is even more visible in the momentum-space correlations discussed in Sec. V B: A HB-T effect is responsible for strong bunching correlations between neighboring momentum states. The peak value of these correlations is fixed by the Gaussian statistics to the usual HB-T value; the momentum-space linewidth displays interesting behaviors as a function of temperature and momentum, which can be related to the overall size of the condensed and thermal components of the cloud. Similar features are also found in the momentum-space linewidth of the correlation between opposite momentum states. Conclusions are finally drawn in Sec. VI.

II. THE PHYSICAL SYSTEM AND THE BOGOLIUBOV DESCRIPTION

In this first section, we introduce the physical system under investigation and we review the basic concepts of the Bogoliubov approach that we use in the following. The experienced reader can go straight to Sec. II D, where we focus on some intriguing yet less known features of the Bogoliubov modes that are important for the following investigation of the two-body correlations.

A. The physical system

We consider an ensemble of Bose atoms of mass m, pairwise interacting via an effective contact potential $g\delta(\mathbf{r})$. This describes the low-energy limit of the bare two-body interaction and depends on the scattering length $a_{\rm sc}$ through the coupling strength $g = 4\pi\hbar^2 a_{\rm sc}/m$. As mentioned in the introduction, for our study it is crucial to be able to access large system sizes so to maximize the selectivity in momentum space. Rather than dealing with the technical complexity of three-dimensional calculations, it is useful to focus on one-dimensional (1D) geometries. To this purpose, we assume that the atoms are confined by an external potential $V_{\rm ext}(\mathbf{r})$ which is tightly confined in the transverse y, z plane at a frequency $\omega_\perp$ larger than the chemical potential and the kinetic and interaction energies. In this way, the atomic sample behaves effectively as a quasi-one-dimensional (quasi-1D) gas [20].

Under this condition, the many-body field operator $\hat\Psi(\mathbf{r})$ can be factorized as $\hat\Psi(\mathbf{r}) = \chi(r_\perp)\hat\Phi(x)$, where $\chi(r_\perp)$ is the wave function in the radial $r_\perp = (y^2+z^2)^{1/2}$ direction and $\hat\Phi(x)$ is the field operator in the longitudinal x direction. By integrating over the transverse degrees of freedom, we get an effective 1D Hamiltonian in the form

$$\hat H = \int dx\, \hat\Phi^\dagger(x)\Big[\hat h + \frac{g_{\rm 1D}}{2}\hat\Phi^\dagger(x)\hat\Phi(x)\Big]\hat\Phi(x). \tag{1}$$

Here, the single-particle Hamiltonian $\hat h = -(\hbar^2/2m)\partial_x^2 + V_{\rm ext}(x)$ includes the kinetic energy along x and the confining potential along this direction, $V_{\rm ext}(x) = \frac{1}{2}m\omega_x^2 x^2$. The following term describes interparticle interactions whose strength $g_{\rm 1D} = 2a_{\rm sc}\hbar\omega_\perp$ is the effective quasi-1D interaction constant for a cylindrically symmetric trap of frequency $\omega_\perp$ [20].

B. The Bogoliubov approximation

Following the number-conserving Bogoliubov formalism developed in Refs. [25,26], we split the field operator $\hat\Phi(x,t)$ into the *condensed* component describing atoms occupying the single-particle condensate state and the *noncondensed* component that accounts for the population of the excited single-particle states,

$$\hat\Phi(x) = \Phi_0(x)\hat a_0 + \delta\hat\Phi(x). \tag{2}$$

Here the operator $\hat a_0$ annihilates a particle from the condensate mode $\Phi_0(x)$, while $\delta\hat\Phi(x)$ annihilates a noncondensed particle at position x. The process by which a particle is transferred from the noncondensed into the condensate component is described by the action of the operator $\hat\Lambda(x)$, defined as

$$\hat\Lambda(x) = \frac{1}{\sqrt{N}}\hat a_0^\dagger\,\delta\hat\Phi(x). \tag{3}$$

Here N is the total number of particles, which differs from the (average) number of condensate atoms $N_0 \equiv \langle\hat a_0^\dagger\hat a_0\rangle$ by the amount $\delta N \equiv \int dx\,\langle\hat\Lambda^\dagger(x)\hat\Lambda(x)\rangle$. In contrast to many treatments of low-dimensional gases, in this work we do not adopt the density or phase representation and we stick to the native form of the field operators $\hat\Phi(x)$ for which momentum

space observables are readily obtained by means of Fourier transforms. Of course, this restricts our discussion to true condensates with long-range order.

In the weakly interacting limit where $N \to \infty$ and $g_{1D} \to 0$ at a fixed mean-field energy Ng_{1D}, one has $\delta N \approx 1$ and one can adopt a perturbative approach in $\delta N/N$. Note that in this limit the chemical potential μ remains constant as it is related to the product Ng_{1D}, while the critical temperature for condensation is pushed to high temperatures (strictly speaking to infinity) and the characteristic coherence length of the quasicondensate also grows. This supports our neglect of quasicondensate effects.

The Gross-Pitaevskii theory accounts for the zeroth-order term of this expansion, while the Bogoliubov theory of noninteracting excitations living on top of the condensate accounts for the first-order correction. At the lowest nontrivial level in this perturbative expansion, the time evolution of $\hat{\Lambda}(x,t)$ and of its Hermitian conjugate $\hat{\Lambda}^\dagger(x,t)$ is governed by the Bogoliubov–de Gennes equations [25]

$$i\hbar\frac{d}{dt}\begin{pmatrix}\hat{\Lambda}\\ \hat{\Lambda}^\dagger\end{pmatrix} = \mathcal{L}\begin{pmatrix}\hat{\Lambda}\\ \hat{\Lambda}^\dagger\end{pmatrix} = \begin{pmatrix}L_{QQ} & L_{QQ^*}\\ L_{Q^*Q} & -L_{QQ}\end{pmatrix}\begin{pmatrix}\hat{\Lambda}\\ \hat{\Lambda}^\dagger\end{pmatrix}, \tag{4}$$

where the (operator-valued) components of the Bogoliubov operator $\mathcal{L}$ are defined as

$$L_{QQ} = [H_{\rm GP} + Ng_{1D}\,Q|\Phi_0(x,t)|^2 Q - \mu], \tag{5a}$$

$$L_{QQ^*} = Ng_{1D}\,Q\Phi_0^2(x,t)Q^*, \tag{5b}$$

$$L_{Q^*Q} = (L_{QQ^*})^*. \tag{5c}$$

At this level of approximation, in Eq. (5a), $\Phi_0(x)$ coincides with the (normalized) ground-state solution of the Gross-Pitaevskii equation [20] and $H_{\rm GP} = -\hbar^2\partial_x^2/2m + Ng_{1D}|\Phi_0(x,t)|^2 + V_{\rm ext}(x)$ is the Gross-Pitaevskii Hamiltonian. We denote the Thomas-Fermi radius of the Gross-Pitaevskii ground state by $L_{\rm bec}$ in the following. In Eqs. (5a)–(5c), the operator $Q \equiv \mathbb{I} - |\Phi_0\rangle\langle\Phi_0|$ is the projector onto the noncondensed component, that is, onto the Hilbert subspace spanned by all single-particle excited states.

C. The Bogoliubov Hamiltonian and its ground state

The $\hat{\Lambda}(x)$ operator can be conveniently expressed in the basis of the Hilbert space composed by the positive norm and positive frequency eigenvectors $[u_n(x), v_n(x)]^T$ (with $n \in \mathbb{N}$) of $\mathcal{L}$ and the associated negative norm and negative frequency ones $[v_n^*(x), u_n^*(x)]^T$ [22,25]. In terms of this basis, we can expand the noncondensed operators as

$$\hat{\Lambda}(x) = \sum_{n\in(+)}(\hat{b}_n u_n(x) + \hat{b}_n^\dagger v_n^*(x)), \tag{6}$$

where the sum runs over the positive norm modes only. Note that for a trapped condensate, all $u_n(x)$ and $v_n(x)$ can be taken as real.

By combining this expansion with the decomposition Eq. (2) of the field operator, the Hamiltonian of the system in Eq. (1) can be conveniently written, to order $O(1)$ in the particle number N, in the diagonal form

$$\hat{H} = E_0(N) + \sum_n E_n\hat{b}_n^\dagger\hat{b}_n, \tag{7}$$

where $E_0(N)$ is the ground-state energy (see Eq. (71) in Ref. [25] for the explicit form). The $\hat{b}_n$ and $\hat{b}_n^\dagger$ operators satisfy bosonic commutation rules, $[\hat{b}_m, \hat{b}_n^\dagger] = \delta_{m,n}$, and physically correspond to the destruction and creation of quanta of excitation in the different excitation modes of the condensate. The Bogoliubov ground state $|0\rangle_{\rm bog}$ is the (unique) state that is annihilated by all quasiparticle operators $\hat{b}_n$,

$$\hat{b}_n|0\rangle_{\rm bog} = 0 \qquad \forall n. \tag{8}$$

The Bogoliubov ground state $|0\rangle_{\rm bog}$ is different from $|\Phi_0\rangle$ in that it contains an admixure of (noncondensed) single-particle excited states, which are referred to as the *quantum depletion*. Note that the Bogoliubov theory does not include terms beyond quadratic order in the Hamiltonian (7), which physically means that the different excitation modes are assumed to be not interacting.

D. The Bogoliubov modes of a trapped condensate

In the Bogoliubov approximation, the structure of the excitations of a trapped condensate are readily obtained by diagonalizing the Bogoliubov operator (4). We have numerically diagonalized the Bogoliubov operator on a one-dimensional lattice of $\mathcal{N}_p$ points uniformly spaced by $dx = L/\mathcal{N}_p$. The kinetic energy is implemented by evaluating the spatial second derivative via a fourth-order finite difference scheme [27]. Care has been paid to ensure convergence of the results on the IR side against the integration box size L and on the UV side against the lattice spacing dx. This diagonalization provides us with both the eigen-energies (i.e., the spectrum) and the eigenmodes (i.e., the Bogoliubov excitations modes) that we now briefly describe.

In Fig. 1(a), we report the numerical result for the spectrum of the Bogoliubov operator $\mathcal{L}$ for a harmonically trapped condensate of chemical potential $\mu = 11.2\,\hbar\omega_x$. We compare it with the analytical solutions obtained in the Thomas-Fermi (red dashed) and noninteracting (blue dot-dashed) limits. The former reproduces well the low-energy modes of *collective*—phononic—nature. The latter recovers the high-energy part of the spectrum, where modes have a *single-particle* nature [20,22]. The crossover between the two regimes is set by the interaction energy $\mu \simeq g_{1D}n(0)$, where $n(x) \equiv N|\Phi_0(x)|^2$ is the condensate density.

In Figs. 1(b) and 1(c), we show the numerical results for a few of the functions $u_n(x)$ and $v_n(x)$ associated with the two types of Bogoliubov excitation modes. We have plotted the solutions for the $n = 1$, 10, 30 modes of energy $E_{1,10,30} \simeq 1$, 8.59, $26.0\,\hbar\omega_x$. These values were chosen to highlight the structure of the Bogoliubov modes in the *collective* ($n = 1$), intermediate ($n = 10$), and *single-particle* ($n = 30$) part of the energy spectrum. At low energies, i.e., small values of n, where the excitations have a *collective* nature, the u_n, v_n have similar amplitudes. In the opposite regime of *single-particle* excitations, i.e., at large values of n, the amplitude of the v_n tends to vanish while that of the u_n remains almost unaffected.

Also, the spatial profiles of both the u_n and v_n functions change drastically with n. These modifications are central to understanding the structure of the two-body correlations that we are going to discuss in the next sections. More specifically, the $u_n(x)$ and $v_n(x)$ functions of low-energy modes [e.g., the

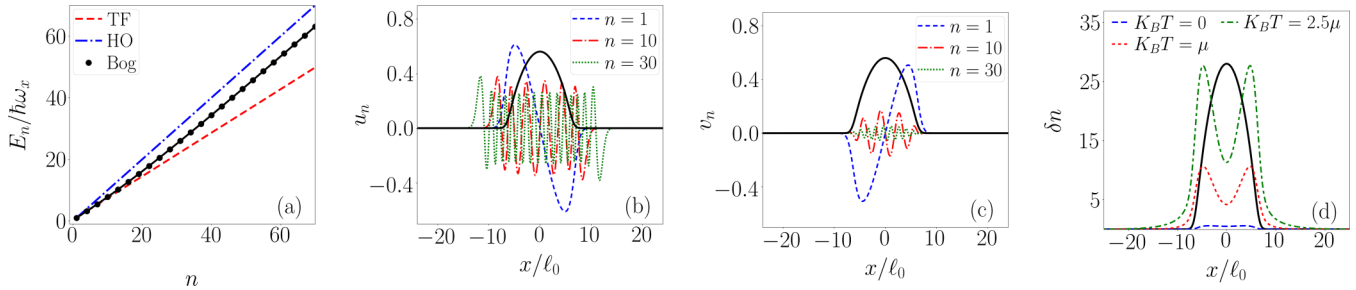

FIG. 1. (a) Bogoliubov spectrum in a one-dimensional condensate in the Thomas-Fermi regime with $\mu/\hbar\omega_x = 11.2 \gg 1$. Numerical (black), hydrodynamic Thomas-Fermi limit (dashed red), and harmonic oscillator (dot-dashed blue) predictions for the spectrum of excitation modes as a function of the mode label n. [(b), (c)] Spatial profiles of the $u_n(x)$ and $v_n(x)$ functions for the $n = 1$ (dashed blue line), $n = 10$ (dot-dashed red line), and $n = 30$ (dotted green line) modes of energies $E_{1,10,30} \simeq 1,\ 8.59,\ 26.0\,\hbar\omega_x$. (d) Density of the noncondensed atoms δn for three different temperatures, $K_BT = 0$ (dashed blue line), $K_BT = \mu$ (dotted red line), and $K_BT = 2.5\mu$ (dot-dashed green line). The black solid line in panels [(b)–(d)] depicts the spatial profile $|\Phi_0(x)|^2$ of the condensate [in units of ℓ_0^{-1} in panels (b) and (c) and in arbitrary units in panel (d) for readability's sake]. The plotted data have been obtained by diagonalizing the Bogoliubov operator in Eg. (4) in the text, on a grid of $\mathcal{N}_p = 2048$ points and an integration box of size $L = 80\ell_0$. Here, $\ell_0 = \sqrt{\hbar/2m\omega_x}$ is the harmonic oscillator length.

blue dashed line for the $n = 1$ dipole mode in Figs. 1(b) and 1(c)] have a similar shape and are localized within the condensate (whose density profile is indicated by the black solid line). This is because the *collective* character of low-energy modes requires the presence of the underlying condensate. In the opposite regime of large energies and *single-particle* excitations, the spatial extensions of the $u_n(x)$ and $v_n(x)$ strongly differ from one another. On the one hand, the functions $u_n(x)$ of high-energy modes [e.g., the green dotted line for $n = 30$ in Fig. 1(b)] display a standing-wave profile with a relatively uniform envelope which extends well beyond the density profile of the condensate. This is because highly energetic single particles can freely climb along the sides of the harmonic trap outside the condensate. On the other hand, the $v_n(x)$ functions [red dash-dotted and green dotted lines in Fig. 1(c)] have a significantly nonzero value only in the condensate region. The envelope of their standing-wave profile smoothly reaches the condensate edge but is largest around the trap center: This feature can be ascribed to the nonhomogeneous density profile of the condensate and to the way the collective or single-particle character of a mode is related to the local density: In a trap, a given excitation mode of frequency ω has a more collective nature and thus a larger $v_n(x)$ in the central high-density region where the local interaction energy $g_{1D}n(x)$ is larger.

As a final remark, we show in Fig. 1(d) the spatial profile of the noncondensed fraction given, to order $O(1)$, by

$$\delta n(x) = \langle \hat{\Lambda}^\dagger(x)\hat{\Lambda}(x)\rangle. \tag{9}$$

First of all, the total number of noncondensed particles increases with the temperature, as expected because the temperature promotes particles outside the ground state. While the quantum depletion at $T = 0$ is relatively flat up to the edge of the condensate, the thermal component visible at higher T's extends well beyond the condensate and is suppressed at the center of the trap by the repulsive effect exerted by the condensate [see the extra term $\sim|\Phi_0(x)|^2$ in Eq. (5a)].

III. TWO-BODY CORRELATIONS: GENERAL THEORY

After having reviewed the basic concepts of the Bogoliubov theory and presented the spatial structure of the excitation modes in a harmonically trapped geometry, we are now in a position to attack the core problem of this work, namely the two-body correlations in both the position and momentum space. In this section, we outline the approach to calculate the correlation functions in the Bogoliubov approximation.

To maintain full generality at this stage, we consider a generic two-body correlation function of the form

$$G^{(2)}(s_1, s_2) = \langle \hat{\Phi}^\dagger(s_1)\hat{\Phi}^\dagger(s_2)\hat{\Phi}(s_2)\hat{\Phi}(s_1)\rangle, \tag{10}$$

where s_1 and s_2 are generic variables either in the position or the momentum space.

Up to terms of order $O(1)$ of the Bogoliubov expansion in powers of the particle number N, Eq. (10) can be expanded as

$$G^{(2)}(s_1, s_2) = N^2\, G^{(2)}_{\Phi_0\Phi_0}(s_1, s_2) + N\, G^{(2)}_{\Phi_0\Lambda}(s_1, s_2) + G^{(2)}_{\Lambda\Lambda}(s_1, s_2), \tag{11}$$

where the terms proportional to $G^{(2)}_{\Phi_0\Phi_0}(s_1, s_2)$, $G^{(2)}_{\Phi_0\Lambda}(s_1, s_2)$, and $G^{(2)}_{\Lambda\Lambda}(s_1, s_2)$ are of different orders in N and account for different type of correlations. The first term $G^{(2)}_{\Phi_0\Phi_0}$

$$G^{(2)}_{\Phi_0\Phi_0}(s_1, s_2) = |\Phi_0(s_1)|^2\,|\Phi_0(s_2)|^2 \tag{12}$$

describes the trivial correlations between particles in the condensate. Thermal and quantum fluctuations are captured by the following terms. The second term is proportional to

$$G^{(2)}_{\Phi_0\Lambda}(s_1, s_2) = [-|\Phi_0(s_1)|^2|\Phi_0(s_2)|^2 + (|\Phi_0(s_1)|^2\langle\hat{\Lambda}^\dagger(s_2)\hat{\Lambda}(s_2)\rangle + |\Phi_0(s_2)|^2\delta\langle\hat{\Lambda}^\dagger(s_1)\hat{\Lambda}(s_1)\rangle).$$
$$+.\,(\Phi_0^*(s_1)\Phi_0^*(s_2)\langle\hat{\Lambda}(s_2)\hat{\Lambda}(s_1)\rangle + \Phi_0^*(s_1)\Phi_0(s_2)\langle\hat{\Lambda}^\dagger(s_2)\hat{\Lambda}(s_1)\rangle + \text{c.c.})] \tag{13}$$

and involves particles in and out of the condensate. Here, "c.c." indicates the complex conjugation operation. The third term is proportional to

$$G^{(2)}_{\Lambda\Lambda}(s_1, s_2) = \langle \hat{\Lambda}^\dagger(s_1)\hat{\Lambda}^\dagger(s_2)\hat{\Lambda}(s_2)\hat{\Lambda}(s_1)\rangle, \tag{14}$$

and describes correlations between the noncondensed particles.

In the position space, the correlation function that we are considering is physically related to the correlation function of the density fluctuations, namely the connected component of the density-density correlation function

$$G^{(2)}_{\rm c}(x_1, x_2) = \langle : \hat{n}(x_1)\hat{n}(x_2) : \rangle - \langle \hat{n}(x_1)\rangle\langle \hat{n}(x_2)\rangle \, . \tag{15}$$

Depending on whether the $x_{1,2}$ points are chosen inside or outside the spatial region occupied by the condensate, different contributions to the fluctuations will dominate. The $G^{(2)}_{\Phi_0\Lambda}$ is of higher order in N and thus generally larger, but it quickly becomes negligible when at least one of the two points $x_{1,2}$ is moved outside the condensate. In this case, the leading contribution is the $G^{(2)}_{\Lambda\Lambda}$ one.

In the momentum space, there is again a clear separation of scales between the condensate that lives in low-momentum states up to $k \simeq 1/L_{\rm bec}$ and the noncondensed fraction that extends up to much higher momenta determined by the temperature or the inverse healing length of the condensate. This separation allows us to separately identify the three terms in Eqs. (12)–(14). The correlations that are of interest for the present work involve modes at k_1, k_2 located outside the condensate and are described by the highest order $G^{(2)}_{\Lambda\Lambda}(k_1, k_2)$ term. In the rest of this work, we will focus on this term for the momentum-space correlations.

The second-order correlators appearing in $G^{(2)}_{\Phi_0\Lambda}(s_1, s_2)$ involve products of respectively the *normal* and *anomalous* averages of the Bogoliubov operator:

$$G^{(1)}(s_1, s_2) = \langle \hat{\Lambda}^\dagger(s_1)\hat{\Lambda}(s_2)\rangle, \tag{16}$$

$$A^{(1)}(s_1, s_2) = \langle \hat{\Lambda}(s_1)\hat{\Lambda}(s_2)\rangle. \tag{17}$$

Given the quadratic form of the Bogoliubov Hamiltonian, the thermal equilibrium state has a Gaussian form at any temperature and the Wick expansion is exact. As a consequence, the quartic correlator $G^{(2)}_{\Lambda\Lambda}(s_1, s_2)$ in Eq. (14) can be expanded in terms of products of the second-order correlators as

$$G^{(2)}_{\Lambda\Lambda}(s_1, s_2) = G^{(2)}_{\Lambda\Lambda,\rm N}(s_1, s_2) + G^{(2)}_{\Lambda\Lambda,\rm A}(s_1, s_2), \tag{18}$$

where

$$G^{(2)}_{\Lambda\Lambda,\rm N}(s_1, s_2) = |G^{(1)}(s_1, s_2)|^2 + G^{(1)}(s_1, s_1)G^{(1)}(s_2, s_2), \tag{19}$$

$$G^{(2)}_{\Lambda\Lambda,\rm A}(s_1, s_2) = |A^{(1)}(s_1, s_2)|^2. \tag{20}$$

In position space, we can make use of the expansion in Eq. (6) to write these expectation values in terms of the Bogoliubov modes as

$$G^{(1)}(x_1, x_2) = \sum_n [(1 + N_n)v_n(x_1)v_n(x_2) + N_n u_n(x_1)u_n(x_2)], \tag{21}$$

$$A^{(1)}(x_1, x_2) = \sum_n [(1 + N_n)u_n(x_1)v_n(x_2) + N_n v_n(x_1)u_n(x_2)], \tag{22}$$

where

$$N_n = \frac{1}{e^{\beta\hbar\omega_n} - 1} \tag{23}$$

is the thermal occupation of the excitation mode of frequency ω_n.

Analogous expressions can be straightforwardly written in the momentum space by defining the Fourier transforms of the Bogoliubov mode functions $u_n(k)$ and $v_n(k)$

$$[u_n, v_n](k) = \frac{1}{\sqrt{L}} \int dx \, [u_n, v_n](x) \, e^{-ikx}, \tag{24}$$

where L is the size of the integration box. These become

$$G^{(1)}(k_1, k_2) = \sum_n [(1 + N_n)v^*_n(k_1)v_n(k_2) \tag{25}$$

$$+ N_n u^*_n(k_1)u_n(k_2)], \tag{26}$$

$$A^{(1)}(k_1, k_2) = \sum_n [(1 + N_n)u_n(k_1)v_n(k_2) \tag{27}$$

$$+ N_n v_n(k_1)u_n(k_2)] \tag{28}$$

and can be directly used to evaluate $G^{(2)}_{\Lambda\Lambda}(k_1, k_2)$ using (18).

IV. TWO-BODY CORRELATIONS IN A SPATIALLY HOMOGENEOUS SYSTEM

As a first application of this approach, in this section we consider the simplest case of a homogeneous system of density n_0 and finite spatial size L with periodic boundary conditions, for which an analytical solution to the Bogoliubov problem in Eq. (4) is available.

Thanks to the translation invariance of the system, solutions for $u_k(x)$ and $v_k(x)$ in a plane-wave form can be found with $u_k(x) = L^{-1/2}\, u_k \, \exp(ikx)$, $v_k(x) = L^{-1/2}\, v_k \, \exp(ikx)$, and

$$u_k = \sqrt{\frac{1}{2}\left(\frac{\xi_k}{\epsilon_k} + 1\right)}, \qquad v_k = -\sqrt{\frac{1}{2}\left(\frac{\xi_k}{\epsilon_k} - 1\right)}. \tag{29}$$

Here, we have used the shorthand notation $\xi_k = \epsilon^0_k + n_0 g_{1D}$, $\epsilon_k = \sqrt{\xi_k^2 - (n_0 g_{1D})^2}$, and $\epsilon^0_k = \hbar^2 k^2/2m$.

In position space, the order $O(N)$ term of the correlation function is proportional to

$$G^{(2)}_{\Phi_0\Lambda}(x_1, x_2) = -\frac{n_0}{L} + \frac{n_0}{L}\sum_{k\neq 0}\{(e^{ik(x_1-x_2)} + e^{-ik(x_1-x_2)}) \times [(u_k + v_k)^2(1 + 2N_k) - 1]\}, \tag{30}$$

where we have exploited the condition $N_k = N_{-k}$ imposed by the inversion symmetry of the system. Here, the first $-n_0/L$ term arises because of the fixed number of atoms N that are in the system and corresponds to the first term in Eq. (13). In the homogeneous geometry where the condensate occupies all the space, the following $O(1)$ term $G^{(2)}_{\Lambda\Lambda}$ is not relevant for the spatial correlation function.

In the momentum space, the condensate only occupies the $k = 0$ state, so for any finite value of k the correlation signal is given by the $G^{(2)}_{\Lambda\Lambda}(k_1, k_2)$ term. The latter can be decomposed in a normal and anomalous part according to (18). The normalized normal correlation takes the form

$$g^{(2)}_{\Lambda\Lambda,\mathrm{N}}(k_1, k_2) \equiv \frac{G^{(2)}_{\Lambda\Lambda,\mathrm{N}}(k_1, k_2)}{G^{(1)}(k_1, k_1)G^{(1)}(k_2, k_2)} = 1 + \delta_{k_1 k_2} \frac{\left|N_{k_1} u^2_{k_1} + (1 + N_{k_1}) v^2_{k_1}\right|^2}{G^{(1)}(k_1, k_1)G^{(1)}(k_2, k_2)} = 1 + \delta_{k_1 k_2}. \tag{31}$$

In a spatially homogeneous configuration, the populations of the different momentum components are in fact independent, so this correlation function differs from unity only for $k_1 = k_2$. Its peak value on the diagonal is equal to 2, as typical for thermal states. This is also true for the case of the quantum depleted atoms at $T = 0$, as first noticed in Ref. [21] and explained in the following. In the next section, we will see how this bunching peak broadens in a trapped geometry, while keeping a maximum value equal to 2.

Analogously, the normalized anomalous correlation function is written as

$$g^{(2)}_{\Lambda\Lambda,\mathrm{A}}(k_1, k_2) \equiv \frac{G^{(2)}_{\Lambda\Lambda,\mathrm{A}}(k_1, k_2)}{G^{(1)}(k_1, k_1)G^{(1)}(k_2, k_2)} = \frac{|(1 + 2N_{k_1})u_{k_1} v_{k_2}|^2}{G^{(1)}(k_1, k_1)G^{(1)}(k_2, k_2)} \delta_{k_1, -k_2}, \tag{32}$$

which is different from zero only for $k_1 = -k_2$. This condition can be physically understood from the properties of the quantum depletion underlying the anomalous correlation at $T = 0$: Since the particles belonging to the quantum depletion form a coherent state of pairs of particles at opposite momenta virtually ejected out of the condensate by the interactions, the anomalous correlations are nonzero only for $k_1 = -k_2$.

In contrast to the normal correlations, the peak value of $g^{(2)}_{\Lambda\Lambda,\mathrm{A}}(k_1, k_2)$ for $k_1 = -k_2$ has a nontrivial k dependence. In particular, since $u_k \to 1$ and $v_k \to 1/[2(\xi k)^2] \to 0$ in the $k \to \infty$ limit [according to Eqs. (29)], the peak correlation diverges for $k \to \infty$. In the simplest $T = 0$ case, one has $N_k = 0$ and thus $g^{(2)}_{\Lambda\Lambda,\mathrm{A}}(k, -k) \to 4(\xi k)^4$. In the more general $T > 0$ case, the large-k divergence has the same form, but it is visible only at high enough values of the momentum for which $N_k \lesssim 1$. Also, in this case, the finite spatial extension of the condensate results in a broadening of this correlation feature.

V. TWO-BODY CORRELATIONS IN A HARMONICALLY TRAPPED SYSTEM

The detailed review of the spatially homogeneous case presented in the previous section paves the way for the study of the correlations in the harmonically trapped system that we are now going to explore. In Sec. V A, we investigate the position space two-body correlations. In Sec. V B, we provide an in-depth study of the momentum-space correlations.

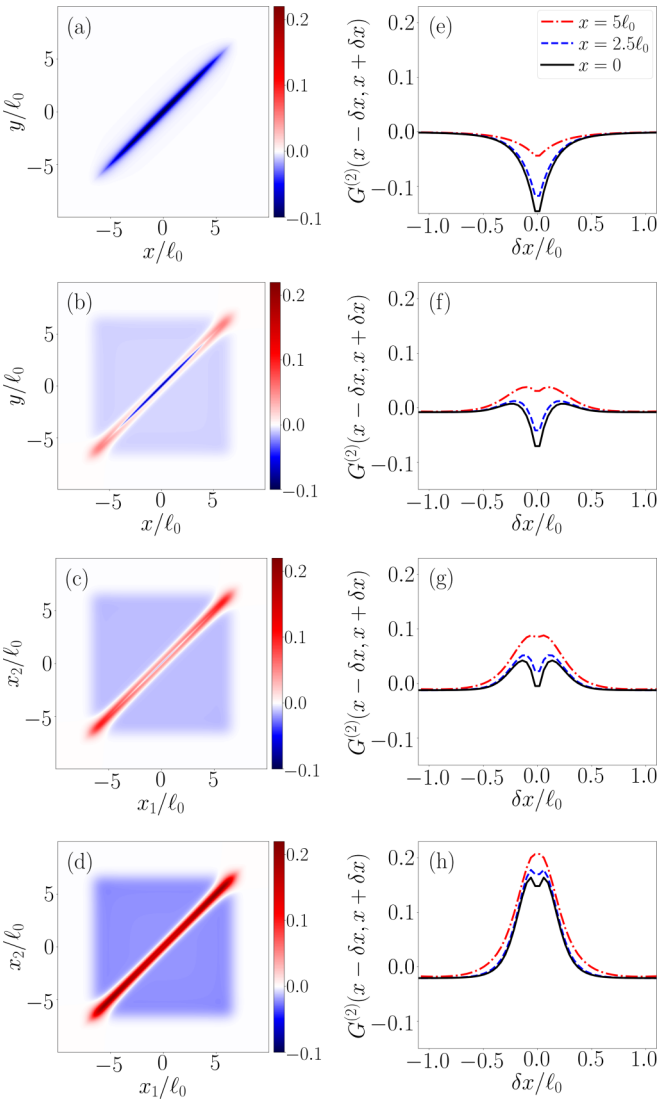

FIG. 2. Numerical solution for the two-body correlation $G^{(2)}_{\Phi\Lambda}(x_1, x_2)$ in real space. The panels [(a)–(d)] on the left column show color plots of this quantity for growing values of the temperature, $K_B T/\mu = 0$, 1, 1.5, 2.5. The panels [(e)–(h)] on the right column show cuts $G^{(2)}_{\Phi\Lambda}(x - \delta x, x + \delta x)$ along straight lines parallel to the antidiagonal located at different spatial positions $x = 0$ (black solid line) $x = 2.5\ell_0$ (blue dashed line), and $x = 5\ell_0$ (red dot-dashed line) for the same values of the temperature. Numerical calculations have been performed on the same grid as in Fig. 1.

A. Position-space correlations

The plots in the different panels of Figs. 2 and 3 illustrate the modification of the density-density correlations captured by the two-body correlation function $G^{(2)}_{\Phi_0\Lambda}(x_1, x_2)$ and $G^{(2)}_{\Lambda\Lambda}(x_1, x_2)$, respectively, in the regions within and outwith the condensate, at increasing values of the temperature.

Let us start from correlations within the condensate. At $T = 0$, a well-contrasted antibunching stripe is visible whose origin reflects the reduced probability of finding two atoms close by because of the repulsive interaction. The typical width of the antibunching stripe is given by the interaction

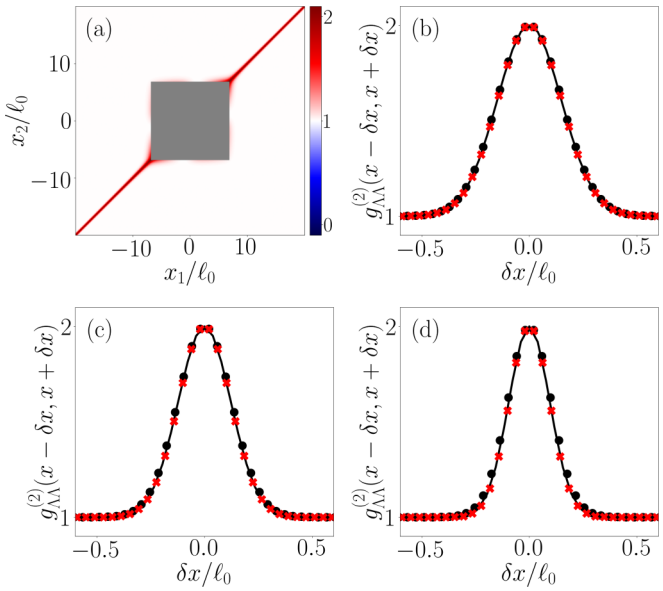

FIG. 3. Numerical solution for the normalized two-body correlation $g^{(2)}_{\Lambda\Lambda}(x_1, x_2)$ in real space. In panel (a), we show the color plot of this quantity for the value of the temperature, $K_BT/\mu = 2.5$. The gray central square, of side $L_{\rm bec} \approx 6.7\ell_0$ equal to the Thomas-Fermi radius, identifies the spatial region where the condensate is located. The panels (b)–(d) show the cuts $g^{(2)}_{\Lambda\Lambda}(x-\delta x, x+\delta x)$ along straight lines parallel to the antidiagonal, at the positions $x = 2L_{\rm bec}$ (black circles) $x = 3L_{\rm bec}$ (continuous lines), respectively, for the values of the temperature: $K_BT = \mu$, $K_BT = 1.5\mu$, and $K_BT = 2.5\mu$. We compare the numerical results with the analytical solution obtained for the classical, noninteracting gas at the same temperature (red crosses). Numerical calculations have been performed on the same grid as in Fig. 1.

strength and is of order the healing length. In the Bogoliubov theory, this feature is accounted for by zero-point vacuum contribution (i.e., for $N_k = 0$) in Eq. (30).

At finite temperature $K_BT/\mu = 1,\ 1.5,\ 2.5$, in contrast, thermal fluctuations induce a bunching associated with their chaotic character. The width of this bunching bump, set by the temperature, is initially broader than the antibunching feature already present at $T = 0$ and gets narrower for growing T. Upon increasing the temperature, the thermal fluctuations of the density therefore progressively overtake the (quantum) antibunching feature. When the temperature is much larger than the interaction energy μ, the bunching ends up dominating over the antibunching dip which is no longer visible [Figs. 2(g) and 2(h)].

The antibunching effect originating from the repulsive interaction and the bunching effect occurring at finite-temperature change differently from one another along the spatial profile of the cloud. As it appears in Figs. 2(e)–2(h), the narrow antibunching dip has a larger amplitude at the center of the cloud (solid black lines) where the density is largest and the effect of repulsive interactions strongest. The inhomogeneous density profile also results in a smaller value of the healing length at the center, and a correspondingly narrower dip in the two-point correlations [Fig. 2(e)]. On the other hand, at low temperatures [Figs. 2(b) and 2(f)], the broad bunching bump starts being visible and has the strongest impact in the spatial region outside the condensate where the thermal atoms are mostly located, as shown in the previous Fig. 1(d). In the bottom panels [Figs. 2(d) and 2(h)] for the highest temperature $k_BT = 2.5\mu$, a substantial thermal component is present also at the trap center, so the overall width of the bunching peak is approximately constant throughout the cloud. Note that the plateau at a slightly negative value that is visible as a bluish uniform area in Figs. 2(a)–2(d) for widely separated positions $x_{1,2}$ is a consequence of the constant number of particles in the system, which fixes the value of the integral of $G^{(2)}(x_1, x_2)$ over the whole space.

As expected, the contribution $G^{(2)}_{\Phi_0\Lambda}$ vanishes when at least one of the two points $x_{1,2}$ lies outside the condensate. In this region, the correlations are then dominated by the higher order $G^{(2)}_{\Lambda\Lambda}$ term. In Fig. 3(a), we report the plot of the (normalized) second-order correlation function

$$g^{(2)}_{\Lambda\Lambda}(x_1, x_2) = \frac{G^{(2)}_{\Lambda\Lambda}(x_1, x_2)}{G^{(1)}(x_1, x_1)G^{(1)}(x_2, x_2)}\,, \tag{33}$$

for a temperature value $K_BT/\mu = 2.5$. A single correlation line appears along the diagonal $x_1 = x_2$, as expected for the cloud of noninteracting particles. Very similar plots are found for other values of the temperature (not shown).

To understand the dependence on the temperature, it is useful to look at the cuts $g^{(2)}_{\Lambda\Lambda}(x-\delta x, x+\delta x)$ along straight lines parallel to the antidiagonal, at different positions. Some such curves are shown in Figs. 3(b)–3(d) for different values of the temperature, $K_BT/\mu = 1,\ 1.5,\ 2.5$. These plots clearly show the position-space HB-T bunching of the thermal cloud, $g^{(2)}_{\Lambda\Lambda}(x, x) = 2$: The spatial extension of the bunching peak is independent on the position and scales with the thermal de Broglie wavelength

$$\lambda_T = \left[\frac{2\hbar}{m\omega_x}\tanh\left(\frac{\hbar\omega_x}{2K_BT}\right)\right]^{1/2}, \tag{34}$$

at the corresponding temperature T. In each panel, the numerical results are compared with the analytical solution obtained for the classical, noninteracting gas at the same temperature,

$$g^{(2)}_{\Lambda\Lambda}(x-\delta x, x+\delta x) = 1 + e^{-4\delta x^2/\lambda_T^2}\,, \tag{35}$$

obtaining an excellent matching between the two curves in this limit.

B. Momentum-space correlations

The plots in Figs. 4(a)–4(c) show examples of the two-body correlations in the momentum-space at different temperatures. In typical experiments [21], these momentum space correlations are extracted as two-body correlations after a long time-of-flight expansion from the source of trapped atoms. In doing this, care must be paid that the signal is not distorted by interaction effects during the time-of-flight expansion. Here, we calculate the normalized contribution that dominates once the momenta k_1 and k_2 are taken outside the condensate region (see Sec. II),

$$g^{(2)}_{\Lambda\Lambda}(k_1, k_2) = \frac{G^{(2)}_{\Lambda\Lambda}(k_1, k_2)}{G^{(1)}(k_1, k_1)\,G^{(1)}(k_2, k_2)}. \tag{36}$$

The condensate region is indicated by the vertical and horizontal gray stripes in Figs. 4(a)–4(c).

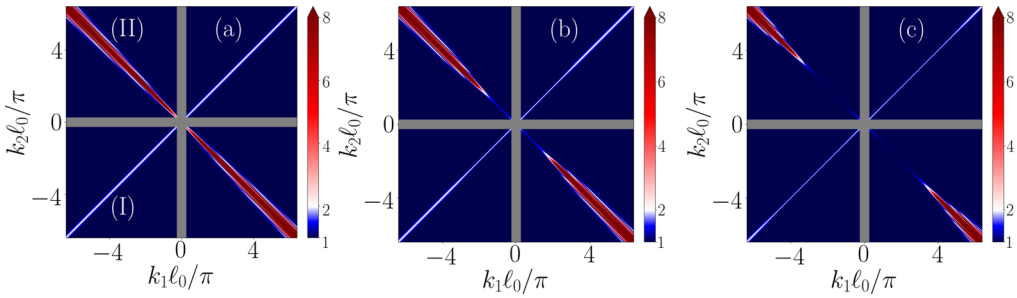

FIG. 4. Numerical results of the two-body correlation function $g^{(2)}_{\Lambda\Lambda}(k_1, k_2)$ in momentum space. Panels (a)–(c) show the profiles of $g^{(2)}_{\Lambda\Lambda}(k_1, k_2)$ for the values of the temperatures $K_BT/\mu = 0$, 1, 2.5. The gray vertical and horizontal stripes, of width $k\ell_0 = 0.5\pi$, identify the region of the momentum space where the condensate contribution to the correlations is located. This region is not relevant for our purposes. We notice the presence of two main features in the two-body correlations in momentum space: (I) the diagonal stripe accounts for the normal contribute $g^{(2)}_{\Lambda\Lambda,\mathrm{N}}(k_1, k_2)$ to the fourth-order correlator, and (II) the antidiagonal stripe accounts instead for the anomalous contribute $g^{(2)}_{\Lambda\Lambda,\mathrm{A}}(k_1, k_2)$ to the fourth-order correlator. Note that the seeming increase of the linewidth of the antidiagonal stripe for large values of $|k_{1,2}|$ is a graphical artifact due to clipping of the color scale at large values of $g^{(2)}_{\Lambda\Lambda}$; see also Eq. (32). Such a clipping was necessary to guarantee readability of all features of the figure.

In analogy with the analytical results discussed in Sec. IV for the homogeneous case, two characteristic features can be identified in these plots: (I) a positive correlation along the $k_1 \approx k_2$ diagonal, due to the normal average of particle-particle correlations $g^{(2)}_{\Lambda\Lambda,\mathrm{N}}(k_1, k_2)$, and (II) a positive correlation along the $k_1 \approx -k_2$ antidiagonal, due to the anomalous average of particle-particle correlations $g^{(2)}_{\Lambda\Lambda,\mathrm{A}}(k_1, k_2)$. In contrast to the homogeneous, infinite case, both these features are here broadened by the finite size of the system. In particular, the k dependence of the linewidth provides detailed information on the microscopic physics of the fluid.

1. Normal averages

The positive correlation signal along the $k_1 \simeq k_2$ diagonal in Figs. 4(a)–4(c) can be interpreted as a HB-T phenomenon. It indeed corresponds to the bunching of bosons with chaotic (thermal) statistics and is characterized by a remarkably uniform value of the peak amplitude $g^{(2)}(k_1, k_2 = k_1) = 2$ for all values of k. This value is in quantitative agreement with the usual HB-T picture, but, as recently pointed out in Ref. [21], the underlying physics is more subtle than the usual HB-T of noninteracting bosons.

The bunching phenomenon results in fact from two distinct contributions, that of the thermally excited Bogoliubov modes (at $T \neq 0$) and that of the quantum depletion in the Bogoliubov ground state. The chaotic character of the statistics associated with those two contributions has a different physical origin. On the one hand, the Bogoliubov excitation modes are noninteracting bosons whose population has a thermal distribution and their statistics is therefore the well-known chaotic (thermal) statistics of ideal bosons. On the other hand, for the quantum depletion, the chaotic character results from the destruction of its quantum coherence when the correlations are probed locally, $k_1 \simeq k_2$, in the momentum space. Indeed, while the quantum depletion is formed by pairs of particles at opposite momenta, the local two-body correlations probe the statistics of particles belonging to two different pairs, discarding the second partner of each particles in a pair.

Even richer is the dependence of the linewidth σ_k of this HB-T peak on the system temperature T and on the specific position in k at which the linewidth is measured. Extending the usual HB-T argument to our more complex configuration, we can anticipate that the width of the bunching peak is inversely proportional to the spatial size of the components that provide the strongest contribution at position k at temperature T. With this general trend in mind, we now turn to the detailed discussion of the numerical results shown in Figs. 5. More specifically, we plot there the root-mean-square width σ_k of the HB-T peak. For any values k and T, σ_k is extracted from the analysis of cuts along the line $k_1 + k_2 = 2k$ in the two-dimensional plots of $g^{(2)}(k_1, k_2)$ at temperature T, like those in Figs. 4(a)–4(c).

a. Temperature dependence. At zero or low temperatures, the width σ_k is dominated by the contribution from the quantum depletion of the condensate. For the relatively large value $\mu/\hbar\omega_x = 11.2$ considered in the figures, the quantum depletion spreads over many Bogoliubov modes of the trapped system. The spatial size of the quantum depletion is determined by the Bogoliubov functions $v_n(x)$ in Eq. (21), which are nonzero only in the region of the condensate. As a consequence, the width σ_k tends to a finite value in the $T \to 0$ limit, inversely proportional to the condensate size L_{bec} (defined as the Thomas-Fermi radius). For the parameters of Fig. 5(a), this corresponds to the value $\sigma_k\ell_0 \approx 0.13$. Quite remarkably, this corresponds to a value of $\sigma_k L_{\mathrm{bec}} \approx 0.9$ which hints at a $1/L_{\mathrm{bec}}$ dependence. This feature will be further investigated in Fig. 6.

On the other hand, at high temperatures the thermal component described by the Bogoliubov functions $u_n(x)$ in Eq. (21) dominates. The spatial size of these functions increases with the mode index n and ends up extending well beyond the condensate size. This provides the decrease of the width σ_k with the temperature T that is visible in Fig. 5(a). More quantitatively, the overall rms size of the thermal cloud of a harmonically trapped noninteracting nondegenerate gas follows a

$$\sigma_x = \sqrt{\frac{k_BT}{m\omega_x^2}} = \ell_0\sqrt{\frac{2k_BT}{\hbar\omega_x}} \tag{37}$$

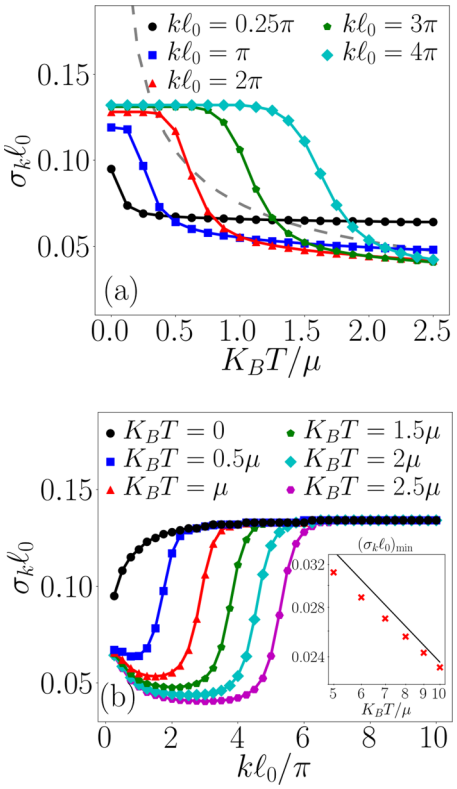

FIG. 5. Numerical results of the normalized two-body correlation function $g^{(2)}_{\Lambda\Lambda}(k_1, k_2)$ in momentum space. Panel (a) shows how the rms of the cuts $g^{(2)}_{\Lambda\Lambda,\mathrm{N}}(k+\delta k, k-\delta k)$ through the diagonal feature varies with the temperature, for the values of $k\ell_0/\pi = 0.25, 1, 2, 3, 4$. At the higher temperatures (and for sufficiently high momentum values so that the Bose-Einstein statistics can be approximated by the Boltzmann one) the curves asymptotically follow the typical $\ell_0\sqrt{2k_BT/\hbar\omega_x}$ dependence of the nondegenerate, harmonically trapped gas (gray-dashed line). Panel (b) shows how the rms of the cuts $g^{(2)}_{\Lambda\Lambda,\mathrm{N}}(k+\delta k, k-\delta k)$ varies with the wave vector k, for the values of the temperature $K_BT/\mu = 0, 0.5, 1, 1.5, 2, 2.5$. The inset shows the scaling with the temperature of the value of the plateau (red markers), compared with the analytical result in Eq. (40) relative to the noninteracting, classical gas.

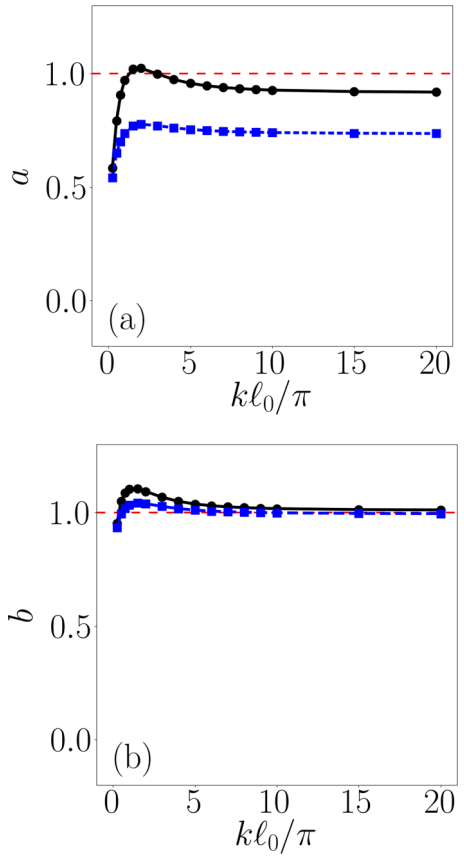

FIG. 6. Scaling of the rms of the cuts $g^{(2)}_{\Lambda\Lambda,\mathrm{N}}(k+\delta k, k-\delta k)$ through the diagonal (black) and $g^{(2)}_{\Lambda\Lambda,\mathrm{A}}(-k+\delta k, k+\delta k)$ through the antidiagonal (blue) features with the size L_{bec} of the condensate at $T = 0$. In panels (a) and (b), we respectively show the exponent b and the prefactor a of the fit of the numerical data with the power law a/L^b_{bec}.

dependence. Taking into account the explicit form of the one-body density matrix of the harmonically trapped, nondegenerate gas [28]

$$\rho^{(1)}(x_1, x_2) = \exp\left[-\frac{m\omega_x^2}{8k_BT}(x_1+x_2)^2\right] \times \exp\left[-\frac{mk_BT}{2\hbar^2}(x_1-x_2)^2\right], \tag{38}$$

where we have assumed that $k_BT \gg \hbar\omega_x$, and transforming this expression to momentum space

$$\rho^{(1)}(k_1, k_2) = \exp\left[-\frac{\hbar^2}{8mk_BT}(k_1+k_2)^2\right] \times \exp\left[-\frac{k_BT}{2m\omega_x^2}(k_1-k_2)^2\right], \tag{39}$$

we obtain the explicit expression

$$\sigma_k = \sqrt{\frac{m\omega_x^2}{8k_BT}} = \frac{1}{\sqrt{8}\,\sigma_x} \tag{40}$$

for the momentum space linewidth [29], which confirms the inverse proportionality on the spatial size of the system expected from the HB-T picture. This curve is displayed here as a dashed line and is found to accurately capture the numerical results for sufficiently high temperatures. The corrections that are visible on the small-k curves are due to the quantum degeneracy of the thermal occupation of the lowest modes.

The two low- and high-temperature regimes are separated by a sharp transition. The position of the transition is determined by the value of the temperature for which the thermal population of the Bogoliubov excitation mode starts dominating over the quantum depletion. As expected, the transition point moves toward higher values of T for growing k since the energy of the Bogoliubov eigenmodes giving the dominant contribution increases with k.

b. Wave-vector dependence. In Fig. 5(b), we plot the width σ_k as a function of the momentum k where it is evaluated for different temperatures. Our interpretation associating the

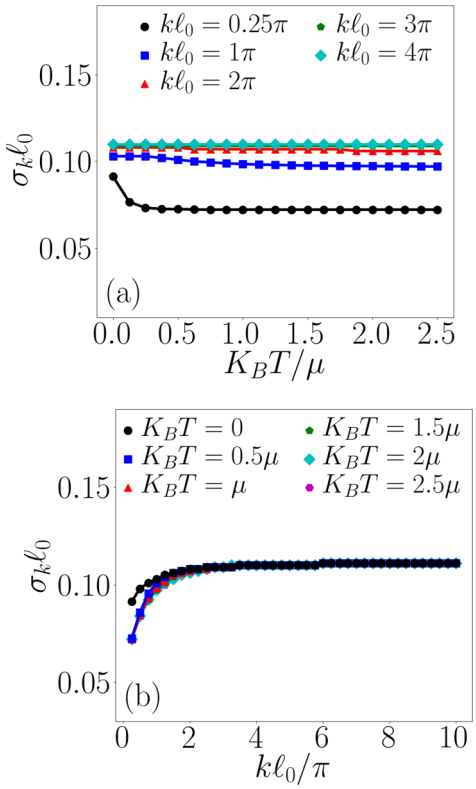

FIG. 7. Numerical results of the normalized two-body correlation function $g^{(2)}_{\Lambda\Lambda}(k_1, k_2)$ in momentum space. Panels (a) and (b) show the rms of the cuts $g^{(2)}_{\Lambda\Lambda,\mathrm{N}}(-k + \delta k, k + \delta k)$ through the antidiagonal feature for the same values of the parameters as in Fig. 5.

HB-T width to the spatial size of the corresponding k component is confirmed. At zero temperature $T = 0$ (black), σ_k slightly increases with the momentum k, which can be interpreted in terms of the stronger localization of the $v_n(x)$ functions of the high-n Bogoliubov modes contributing to the quantum depletion, as shown in Fig. 1(c).

At nonzero temperatures, the curves exhibit a nonmonotonic and richer behavior with k. At large k, all the curves at different temperatures collapse on the $T = 0$ result for σ_k. This happens because the high-k components are not thermally populated as their energy is larger than the temperature, and the only contribution is that from the quantum depletion.

As k decreases, one observes a sharp decrease of σ_k followed by a plateau. This sharp jump corresponds to the sharp transition between the low- and high-temperature regimes identified above in the T-dependent analysis. Indeed, for momenta k whose Bogoliubov energy is sufficiently small for the thermal population to dominate over the quantum depletion, the dominant contribution comes from the $u_n(x)$ functions which extend beyond the condensate and provide a wide thermal cloud of (almost) noninteracting particles as discussed above. This interpretation is confirmed by the close to $1/\sqrt{T}$ scaling of the value of σ_k on the plateau displayed in the inset of Fig. 5(b).

For even smaller values of k, the plateau ends and σ_k displays a slight increase for decreasing k. This feature can be connected to the phononic character of such modes as well as to the corrections to the $\sigma_k \propto 1/\sqrt{T}$ dependence due to the quantum degeneracy of the low-lying noncondensed modes, as already noticed in Fig. 5(a).

c. System-size dependence. To further reinforce our conclusions that the HB-T width σ_k is inversely proportional to the spatial size of the corresponding k component, we now explicitly study the dependence of the width σ_k with the condensate size L_{bec}. In the high-T case, analytical insight on the inverse proportionality on the size of the thermal cloud was provided in Eq. (40). Here, we focus on the bunching of the quantum depletion in the interacting $T = 0$ case, where the condensate size L_{bec} is controlled by varying the strength of interactions, that is, the chemical potential.

For different values of the cut position k, we fit the dependence of σ_k on L_{bec} with a power law of the form a/L^b_{bec}, with the results plotted in Fig. 6 (black line). Except for a relatively small deviation for small values of k, the result in Fig. 6(b) confirms the expected L^{-1}_{bec} dependence for values of $k\ell_0 \gtrapprox 5\pi$. Comparison with Fig. 5(b) shows that this value is comparable to that at which the width σ_k reaches the asymptotic value discussed in the previous section.

2. Anomalous averages

Figure 7 shows an analogous analysis for the positive correlation bump located on the antidiagonal $k_1 + k_2 = 0$. This feature is associated with the anomalous averages and only appears in interacting gases. According to Eq. (22), this feature is determined by the products of $u_n(x)$ and $v_n(x)$ Bogoliubov amplitudes and the overall spatial size is determined by the latter. As we have seen in Fig. 1(c), the $v_n(x)$ roughly follow the condensate shape for all Bogoliubov modes, so we do not expect a marked temperature dependence for the width σ_k. This physical picture is confirmed by the numerical results shown in Fig. 7(a) for different positions k of the cut, which clearly display a much weaker T dependence as compared to the corresponding curves in Fig. 5(a).

The same physics is also visible in the k-dependent curves shown in Fig. 7(b), which feature an analogously weak dependence for all considered temperatures. In contrast to the complex behaviours observed for the diagonal feature studied in Fig. 5(b), the k dependence is here a monotonically growing one and can be again interpreted in terms of the weaker localization of the $v_n(x)$ functions for the lower modes displayed in Fig. 1.

An explicit illustration of the condensate-size dependence at $T = 0$ is provided by the blue curves in Fig. 6. Also in this case, for sufficiently large values of k, the scaling in Fig. 6(b) points to an inverse proportionality of the momentum-space linewidth on the condensate size, $\sigma_k \propto 1/L_{\mathrm{bec}}$. The smaller value of the prefactor a visible in Fig. 6(a) can be interpreted in terms of the dependence of the antidiagonal features on $v_n(x)$, rather than the $v_n(x)^2$ dependence that characterizes the diagonal one.

VI. CONCLUSION

In this work, we have taken inspiration from the recent experiment in Ref. [21] to carry out a detailed study of

the consequences of the spatial inhomogeneity of a harmonically trapped Bose-Einstein condensate on the two-body correlation functions in both position and momentum spaces at low temperatures. To reduce the technical challenge and be able to unravel the basic physics of the system, we have made use of the Bogoliubov description of the weakly interacting gas and we have restricted our attention to the computationally easier one-dimensional geometry. We are, of course, aware that the severe assumptions made in our work prevent us from quantitatively capturing all features of the experiment. Nonetheless, our calculations for an idealized model provide a crucial step in view of unraveling the subtle interplay of the finite spatial size with interaction and temperature effects.

As a first step, we have unveiled intriguing features in the spatial structure of the Bogoliubov excitation modes, which result from a subtle interplay of the inhomogeneous density profile and the collective versus single-particle character of the mode in the different spatial regions. This understanding of the excitation modes provides a crucial tool to investigate the two-body correlations in both the position and the momentum spaces.

In the position space, we find markedly different behaviors in the center of the trap and in the outer region: In the central region, the zero-temperature antibunching due to interactions in the condensate is slowly replaced by bunching of thermal atoms as temperature grows. The outer regions are instead dominated by thermal atoms that show thermal bunching at any finite temperatures.

In the momentum space, two main features are clearly visible in the correlation pattern. On the main diagonal, namely for $k_1 \approx k_2$, a marked Hanbury-Brown and Twiss bunching signal is visible with the normalized correlation function going up to the usual value $g^{(2)} = 2$ of chaotic fields, as experimentally observed in Ref. [21]. Depending on the specific values of the momentum and the temperature under consideration, the origin of this chaotic character is very different, however. For thermally occupied modes, it is related to the Bogoliubov description of the thermal cloud in terms of noninteracting quasiparticles. For modes that are only populated by the quantum depletion, the thermal character originates from tracing out the opposite momentum states with which each state is quantum correlated. This physical difference results in a different scaling of the linewidth of the HB-T bunching feature in different regions of k space at a given temperature: For low-k, thermally occupied modes, this is determined by the inverse spatial size of the thermal cloud; for the high-k modes occupied by the quantum depletion only, the linewidth is determined by the inverse condensate size.

Another bunching feature appears on the antidiagonal for $k_1 \approx -k_2$. This feature is due to the anomalous average of the atomic field operator, that is, the quantum correlation between pairs of opposite momentum atoms forming the quantum depletion. In contrast to the diagonal feature, the antidiagonal one gets monotonically weaker for increasing temperatures without changing its qualitative shape. In all regimes, its linewidth is in fact fixed by the size of the condensate and displays a weak temperature dependence.

Our natural next steps will consist in looking for the $k_1 \approx -k_2$ features and exploiting the k dependence to get deeper insight on the structure of the atomic gas in upgraded experiments along the lines of Ref. [21]. Future theoretical work includes the investigation of correlations in regimes of higher temperatures and/or stronger interactions where excitations can no longer be considered as noninteracting quasiparticles and non-Gaussian corrections to the Bogoliubov theory must be included. All these studies will eventually contribute to establishing Hanbury-Brown and Twiss techniques as a powerful experimental window on the microscopic physics of strongly correlated quantum gases.

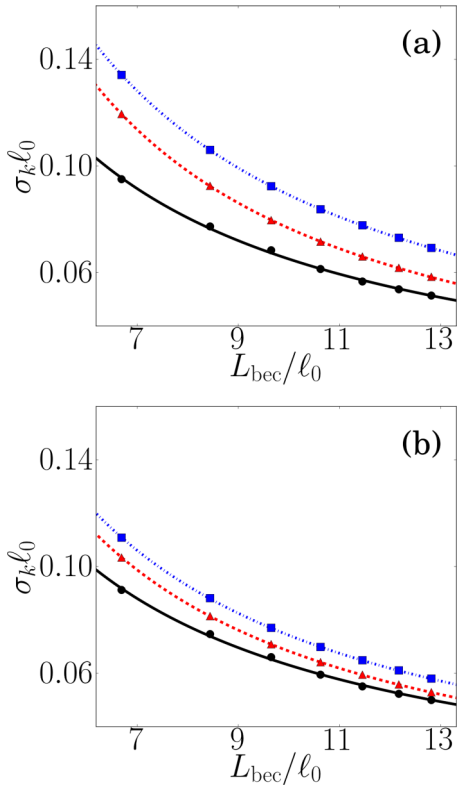

FIG. 8. Scaling of the rms of the cuts (a) $g^{(2)}_{\Lambda\Lambda,N}(k+\delta k, k-\delta k)$ and (b) $g^{(2)}_{\Lambda\Lambda,A}(-k+\delta k, k+\delta k)$ with the size of the condensate, for the value of the temperature $T = 0$. The numerical data (symbols) are compared to the fitted curves (continuous lines), for the values of the wave vectors $k\ell_0/\pi = 0.25,\ 1,\ 10$ (respectively in black dots, red triangles, and blue squares).

ACKNOWLEDGMENTS

S.B. acknowledges funding from the Leverhulme Trust Grant No. ECF-2019-461 and the Lord Kelvin/Adam Smith (LKAS) Leadership Fellowship. I.C. acknowledges funding from Provincia Autonoma di Trento and from the Quantum Flagship Grant PhoQuS (820392) of the European Union. D.C. acknowledges support from the LabEx PALM (Grant No. ANR-10-LABX-0039), the Région Ile-de-France in the framework of the DIM SIRTEQ, the "Fondation d'entreprise iXcore pour la Recherche," the Agence Nationale pour la Recherche (Grant No. ANR-17-CE30-0020-01) and the Institut Universitaire de France.

APPENDIX: FITS FOR THE SCALING OF THE WIDTH OF THE CORRELATION LINES WITH THE SIZE OF THE SYSTEM

In Fig. 8, we show an example of the fits that led to the results reported in Figs. 6(a) and 6(b) in the main paper, respectively, for the scaling of the rms of the diagonal and antidiagonal correlation lines in momentum space, with the size $L_{\rm bec}$ of the system. The discrete points are the numerical data, while the continuous lines are the curves fitting the data according to the power law $a/L_{\rm bec}^{b}$.

[1] R. Loudon, *The Quantum Theory of Light* (Oxford University Press, Oxford, UK, 2000).

[2] D. F. Walls and G. Milburn, *Quantum Optics* (Springer Verlag, Berlin, 2006).

[3] K. Huang, *Statistical Mechanics* (Wiley, New York, 1987).

[4] C. Cohen-Tannoudji, Lectures at Collège de France, 1999–2000 (unpublished), http://www.phys.ens.fr/∼cct/college-de-france/1999-00/1999-00.htm.

[5] J. D. Gunton and M. J. Buckingham, Condensation of the ideal Bose gas as a cooperative transition, Phys. Rev. **166**, 152 (1968).

[6] S. M. Barnett, S. Franke-Arnold, A. S. Arnold, and C. Baxter, Coherence length for a trapped bose gas, J. Phys. B **33**, 4177 (2000).

[7] S. Franke-Arnold, G. Huyet, and S. M. Barnett, Measures of coherence for trapped matter waves, J. Phys. B **34**, 945 (2001).

[8] M. Schellekens, R. Hoppeler, A. Perrin, J. Viana Gomes, A. A. D. Boiron, and C. I. Westbrook, Hanbury-Brown Twiss effect for ultracold quantum gases, Science **310**, 648 (2005).

[9] S. Folling, F. Gerbier, A. Widera, O. Mandel, T. Gericke, and I. Bloch, Spatial quantum noise interferometry in expanding ultracold atom clouds, Nature (London) **434**, 481 (2005).

[10] A. Ottl, S. Ritter, M. Kohl, and T. Esslinger, Correlations and Counting Statistics of an Atom Laser, Phys. Rev. Lett. **95**, 090404 (2005).

[11] A. Perrin, R. Bücker, S. Manz, T. Betz, C. Koller, T. Plisson, T. Schumm, and J. Schmiedmayer, Hanbury Brown and Twiss correlations across the Bose-Einstein condensation threshold, Nat. Phys. **8**, 195 (2012).

[12] R. G. Dall, A. G. Manning, S. S. Hodgman, W. Rugway, K. V. Kheruntsyan, and A. G. Truscott, Ideal n-body correlations with massive particles, Nat. Phys. **9**, 341 (2013).

[13] B. Fang, A. Johnson, T. Roscilde, and I. Bouchoule, Momentum-Space Correlations of a One-Dimensional Bose Gas, Phys. Rev. Lett. **116**, 050402 (2016).

[14] C. Carcy, H. Cayla, A. Tenart, A. Aspect, M. Mancini, and D. Clément, Momentum-Space Atom Correlations in a Mott Insulator, Phys. Rev. X **9**, 041028 (2019).

[15] R. Hanbury Brown and R. Q. Twiss, Test of a new type of stellar interferometer on sirius, Nature (London) **178**, 1046 (1956).

[16] T. Jeltes, J. M. McNamara, W. Hogervorst, W. Vassen, V. Krachmalnicoff, M. Schellekens, A. Perrin, H. Chang, D. Boiron, A. Aspect *et al.*, Comparison of the Hanbury Brown-Twiss effect for bosons and fermions, Nature (London) **445**, 402 (2007).

[17] I. Bloch, J. Dalibard, and W. Zwerger, Many-body physics with ultracold gases, Rev. Mod. Phys. **80**, 885 (2008).

[18] I. Lovas, B. Dóra, E. Demler, and G. Zaránd, Full counting statistics of time-of-flight images, Phys. Rev. A **95**, 053621 (2017).

[19] I. Lovas, B. Dóra, E. Demler, and G. Zaránd, Quantum-fluctuation-induced time-of-flight correlations of an interacting trapped Bose gas, Phys. Rev. A **95**, 023625 (2017).

[20] L. P. Pitaevskii and S. Stringari, *Bose-Einstein Condensation and Superfluidity* (Clarendon Press, Oxford, UK, 2016).

[21] H. Cayla, S. Butera, C. Carcy, A. Tenart, G. Hercé, M. Mancini, A. Aspect, I. Carusotto, and D. Clément, Hanbury-Brown and Twiss Bunching of Phonons and of the Quantum Depletion in a Strongly-Interacting Bose Gas, Phys. Rev. Lett. **125**, 165301 (2020).

[22] Y. Castin , Bose-Einstein condensates in atomic gases: Simple theoretical results, in *Coherent Atomic Matter Waves, Lecture Notes of Les Houches Summer School*, edited by R. Kaiser, C. Westbrook, and F. David (EDP Sciences and Springer-Verlag, Berlin, 2001), pp. 1–136.

[23] L. Mathey, A. Vishwanath, and E. Altman, Noise correlations in low-dimensional systems of ultracold atoms, Phys. Rev. A **79**, 013609 (2009).

[24] E. Toth, A. M. Rey, and P. B. Blakie, Theory of correlations between ultracold bosons released from an optical lattice, Phys. Rev. A **78**, 013627 (2008).

[25] Y. Castin and R. Dum, Low-temperature Bose-Einstein condensates in time-dependent traps: Beyond the (U) symmetry-breaking approach, Phys. Rev. A **57**, 3008 (1998).

[26] C. W. Gardiner, Particle-number-conserving Bogoliubov method which demonstrates the validity of the time-dependent Gross-Pitaevskii equation for a highly condensed Bose gas, Phys. Rev. A **56**, 1414 (1997).

[27] B. Fornberg, Generation of finite difference formulas on arbitrarily spaced grids, Math. Comput. **51**, 699 (1988).

[28] L. D. Landau and E. M. Lifshitz, *Statistical Physics* (Elsevier, Amsterdam, 2013), Vol. 5.

[29] Note that the momentum space linewidth is defined as the rms linewidth for Δk along the $(k - \Delta k, k + \Delta k)$ curve in the (k_1, k_2) plane.